

Tunable magnetic phases in quasi-one-dimensional systems

Alfredo X. Sánchez¹ and Jean-Pierre Leburton^{1,2,*}

¹*Department of Physics and Beckman Institute, University of Illinois at Urbana-Champaign, Urbana, Illinois 61801, USA*

²*Department of Electrical and Computer Engineering,
University of Illinois at Urbana-Champaign, Urbana, Illinois 61801, USA*

There has been considerable debate on the onset of exotic spin phenomena in quantum wires due to enhanced many-body effects caused by the one-dimensional (1D) alignment of charge carriers. We explain various observed spin effects, such as a carrier density-dependent spin-flip in dilute quasi-1D systems and the variability of the spin polarization in quantum point contacts, by using an unrestricted Hartree-Fock approach with a three-dimensional (3D) Coulomb interaction. The model dimensionality is critical in identifying a complex pattern of magnetic phases varying with magnetic field and confinement. In the limit of vanishing magnetic fields, we show the emergence of a degenerate excited state with opposite spin polarization above a confinement-dependent 1D concentration threshold, which is consistent with observations of a conductance plateau at half the conductance quantum $G_0/2 = e^2/h$, even in the absence of spin-orbit interactions.

Quantum wires (QWRs) are nanostructures characterized by two-dimensional (2D) confinement exhibiting electronic modes transverse to the one-dimensional (1D) motion of charge carriers. The existence of these transverse modes has profound consequences on the interaction between carriers and crystal dynamics, as well as amongst carriers themselves, which uncovers a flurry of exciting properties. In the former case, carrier scattering undergoes size effects¹ that affect the transport properties with important technological consequences for device electronics². In the latter case, the 1D alignment of interacting particles enhances Hartree and exchange interactions giving rise to exotic phenomena such as the formation of Wigner localization^{3,4} or Luttinger liquids^{5,6}. During the last two decades, a wide range of experiments stimulated by the observation of a transport anomaly in semiconductor quantum point contacts (QPCs)⁷⁻⁹ and the demonstration of separate spin and charge excitations in QWRs^{10,11} have suggested the existence of spin-related transport or spontaneous spin polarization in 1D systems^{7,12-21}, as opposed to a Kondo-like effect due to the presence of a quasi-bound state^{9,22,23}. A spin-polarized ground state, while forbidden in strictly 1D systems by the Lieb-Mattis theorem²⁴, could be achieved in realistic QWRs and QPCs, since these devices have two- and three-dimensional structures, potentially giving rise to additional phenomena. This has spurred interest in fully-electric manipulation of spin properties in quantum wires and point contacts^{25,26}.

In this article, we show that 1D systems in longitudinal magnetic fields and in the absence of spin-orbit interaction (as, for instance, in a GaAs wire) can sustain a hierarchy of spin configurations depending on carrier concentration, energy and confinement. Specifically, as carrier concentration increases, the electron system in its ground states evolves from a fully spin-polarized state to an unpolarized state with a spin flip. In the limit of vanishing magnetic fields, there exists a concentration threshold above which the electron system exhibits an excited state with degenerate opposite-spin polarization. We also show that this threshold varies as the strength of the confinement is changed. The latter feature is particularly important for the technological application of electrostatically-confined wires for which the spin polarization can be controlled by electrical gating.

Let us consider a wire with its axis of symmetry along the x -axis. Electrons are confined along the y - and z -directions (perpendicular to the wire) by means of a potential $U_{\text{conf}}(y, z)$, which we model as a superposition of two parabolic wells, i.e. $U_{\text{conf}}(y, z) = \frac{1}{2}m^*\omega_y^2 y^2 + \frac{1}{2}m^*\omega_z^2 z^2$. Here, ω_y and ω_z are the strengths of the confinement along the y - and z -directions, respectively, and m^* is the electron effective mass. The wire is placed in a magnetic field $\vec{B} = B_0\hat{x}$ parallel to the axis of the wire, with an associated Zeeman term $U_Z = g\mu_B B_x \sigma$. (g is the effective electron g -factor, $\mu_B = \frac{q\hbar}{2m^*}$ is the Bohr magneton in the wire, q is the electron charge, and σ is equal to $+1/2$ or $-1/2$ for spin-up or spin-down, respectively.) For the sake of simplicity, the spin-orbit interaction is neglected.

The use of the unrestricted Hartree-Fock model in the extreme quantum limit (i.e. when only one subband is populated)²⁷ results in the expression for the energy $E(k_x, \sigma)$ of an electron in terms of its momentum k_x and spin σ (see Supplementary Methods), which reads:

$$E(k_x, \sigma) = \frac{\hbar^2 k_x^2}{2m^*} + \frac{1}{2}\hbar\omega_y + \frac{1}{2}\hbar\omega_z + \frac{1}{4} \left(\frac{\omega_B}{\omega_y} \right) \hbar\omega_B + g\mu_B B_x \sigma + U_{\text{el}}[n_0] + U_{\text{exch}}(k_x, \sigma) \quad (1)$$

Here, $\omega_B = \frac{qB_x}{m^*}$ is the cyclotron frequency, U_{el} is the Hartree term (which accounts for Coulomb repulsion amongst electrons and is proportional to the total concentration n_0) and U_{exch} is the exchange term. U_{el} and U_{exch} depend

on the overlap function $\zeta_{ab}(p)$ which, in turn, is determined by the strength of the lateral confinement and the shape of the electron wavefunction. (See Supplementary Methods.) The pair of two integral equations for $E(k_x, \uparrow)$ and $E(k_x, \downarrow)$ described by Eq. (1) is then solved to yield the spin-dependent concentrations n_σ (n_\uparrow, n_\downarrow) for a fixed total electron concentration $n_0 = n_\uparrow + n_\downarrow$.

At zero temperature, both n_\uparrow and n_\downarrow are associated with a (positive) spin-dependent Fermi wavevector $k_{f(\sigma)} = \pi n_\sigma$, so that the Fermi energy $E_f = E(k_{f(\sigma)}) = E_f(n_\sigma)$. Then, after setting $E_f(n_\uparrow) = E_f(n_\downarrow)$, the relation between n_\uparrow and n_\downarrow can be written in terms of n_0 and $\Delta n_\sigma \equiv n_\sigma - n_0/2$, i.e.

$$\frac{\pi^2}{2} n_0 \Delta n_\sigma + \sigma \frac{qgB_x}{2\hbar} - \frac{q^2 m^*}{64\pi^2 \epsilon \hbar^2} \int_{2\pi(n_0/2 - \Delta n_\sigma)}^{2\pi(n_0/2 + \Delta n_\sigma)} dp \zeta_{ab}(p) = 0 \quad (2)$$

This equation is discussed in more detail in the Supplementary Methods and holds only for $0 \leq |\Delta n_\sigma| \leq n_0/2$, since $0 \leq n_\sigma \leq n_0$. If Eq. (2) yields the solution $\Delta n_{\uparrow(\downarrow)} > n_0/2$, the identity $k_{f(\downarrow(\uparrow))} = \pi n_{\downarrow(\uparrow)}$ is no longer valid because $n_{\downarrow(\uparrow)}$ would then be negative, and thus must be set to zero in order to still satisfy Eq. (1). In this case, $n_{\downarrow(\uparrow)} = n_0$, which corresponds to full spin polarization.

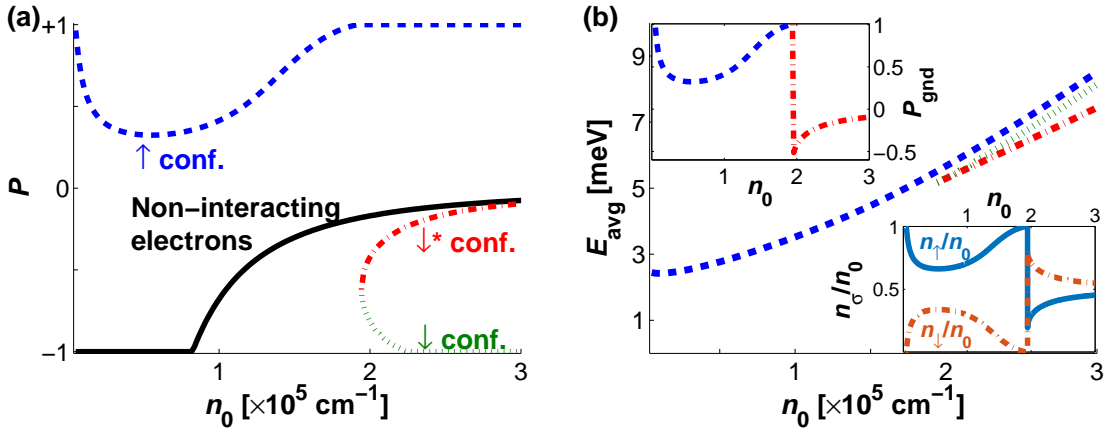


Figure 1. **Spin-polarized regimes.** (a) Polarization $P = (n_\uparrow - n_\downarrow)/n_0$ as a function of the total concentration n_0 at $B_x = 1$ T and $T = 0$ K for non-interacting electrons (solid line) and the three possible polarization configurations for interacting electrons: \uparrow (dashed), \downarrow (dotted) and \downarrow^* (dash-dotted).

In order to illustrate our model, we consider a GaAs quantum wire with $|g| = 0.44$, $m^* = 0.067m_0$ and $\epsilon = 12.9\epsilon_0^{28}$, and where the transverse confinement strength is set to $\hbar\omega_y = \hbar\omega_z = 2.0$ meV. Figure 1(a) shows the polarization $P = (n_\uparrow - n_\downarrow)/n_0$ for interacting and non-interacting electrons, as a function of the total concentration n_0 , at $B_x = 1$ T and zero temperature. The solid line in Figure 1(a) corresponds to the spin polarization for non-interacting electrons, i.e. $\zeta_{ab}(p) = 0$ in Eq. (2). In this case P is negative because of the Zeeman interaction, $U_Z = g\mu_B B_x \sigma$, which lowers the potential energy of spin-down electrons, and hence n_\downarrow exceeds n_\uparrow at the same Fermi energy. For concentrations $n_0 \leq n_B = 0.817 \times 10^5 \text{ cm}^{-1}$, there is complete spin-down polarization and $P = -1$. For n_0 exceeding n_B , one gets $n_\sigma = \frac{n_0}{2} \left[1 - \left(\frac{n_B}{n_0} \right)^2 \text{sign}(gB_x \sigma) \right]$ (as described in the Supplementary Methods), so $P = -\left(\frac{n_B}{n_0} \right)^2$ and $-1 < P < 0$, which corresponds to partial spin-down polarization. As n_0 increases to infinity, P slowly approaches zero. This is due to the fact that the kinetic energy term $T_{x(\sigma)} = \frac{\hbar^2 k_{f(\sigma)}^2}{2m^*} = \frac{\hbar^2 \pi^2 n_\sigma^2}{2m^*}$, which increases with n_σ , contributes predominantly to the total energy at high concentration since U_Z is independent of n_0 . As a result, the Zeeman splitting induced by U_Z becomes insignificant.

The dashed line in Figure 1(a) is one of the solutions to Eq. (1) for interacting electrons, which we call the “ \uparrow ” or “up” configuration, as $P > 0$. For this “ \uparrow ” configuration, the wire is fully spin-polarized when $n_0 \leq n_0^{\text{full}(\text{min})} = 4.51 \times 10^3 \text{ cm}^{-1}$ and $n_0 \geq n_0^{\text{full}(\text{max})} = 1.92 \times 10^5 \text{ cm}^{-1}$. These limiting values are obtained by solving Eq. (2), setting $\Delta n_\uparrow = +n_0/2$. Between those two concentrations, there is partial spin polarization, with a minimum $P = 0.32$ at $n_0 = 0.54 \times 10^5 \text{ cm}^{-1}$. Spin polarization is opposite to the non-interacting case because of the existence of the exchange interaction, which lowers the zero-point energy of the 1D energy subband. At very low n_0 , the exchange energy U_{exch} dominates the kinetic energy T_x , but since $E_f(n_\uparrow) = E_f(n_\downarrow)$, n_\uparrow increases and n_\downarrow decreases (otherwise, $U_{\text{exch}(\downarrow)}$ would be much more negative than $U_{\text{exch}(\uparrow)}$, which would cause $E_f(n_\downarrow)$ to drop far below $E_f(n_\uparrow)$).

For $n_0 \geq n_0^{\text{onset}}$ ($= 1.94 \times 10^5 \text{ cm}^{-1}$), two additional configurations emerge, both with $P < 0$: “ \downarrow ” or “down” (dotted line in Figure 1(a)) and “ \downarrow^* ” or “down-star” (dash-dotted line). In both cases, $P = -0.62$ at the threshold concentration n_0^{onset} , but the two configurations differ as n_0 increases. In the “ \downarrow ” regime, the polarization becomes stronger (i.e. more negative) until the wire is fully polarized ($P = -1$) above $n_0^{\text{full}} = 2.27 \times 10^5 \text{ cm}^{-1}$ (a value also obtained from Eq. (2) with $\Delta n_{\downarrow} = +n_0/2$). Meanwhile, in the “ \downarrow^* ” regime, spin polarization is weakened and tends to zero (approaching the Zeeman splitting for non-interacting electrons) as n_0 goes to infinity. Here we point out that the specific numerical values of the concentrations n_0^{onset} , n_0^{full} , etc., as well as the energies displayed on figures 1-4, are all confinement-dependent and will change for different confinement strengths (see Fig. 5).

The different high-concentration behaviors of the three configurations ($P = 1$, $P = -1$ and $P \rightarrow 0$ for the \uparrow , \downarrow and \downarrow^* configurations, respectively) result from the interplay between the kinetic energy T_x , the exchange interaction U_{exch} and the Zeeman splitting U_Z to satisfy the condition $E_f(n_{\uparrow}) = E_f(n_{\downarrow})$. At high n_0 , U_{exch} dominates U_Z , which can be attenuated in three ways: (1) If n_{\downarrow} is smaller than n_{\uparrow} , which prevents the combined contribution $U_{\text{exch}(\downarrow)} + U_{Z(\downarrow)}$ from becoming too negative; this leads to full spin-up polarization (\uparrow configuration). (2) If n_{\downarrow} is instead larger than n_{\uparrow} , which reduces the kinetic energy term $T_{x(\uparrow)}$ relative to $T_{x(\downarrow)}$, thus lowering $E_f(n_{\uparrow})$ and resulting in full spin-down polarization (\downarrow configuration). (3) If n_{\downarrow} is almost equal to n_{\uparrow} (i.e. $P \rightarrow 0$, just like for non-interacting electrons) in order to balance $T_{x(\downarrow)}$ and $T_{x(\uparrow)}$, since T_x dominates U_{exch} (and U_Z) at high concentrations; this is the behavior of the \downarrow^* configuration.

Whether the electrons in the ground state of the system are in the \uparrow , \downarrow or \downarrow^* configuration depends on which of these three configurations has the lowest energy. Figure 1(b) shows the average energy per electron as a function of n_0 for all three possibilities. If n_0 is above n_0^{onset} , when all three solutions are possible, the \downarrow^* configuration has the lowest energy, with an energy difference with the other two solutions that grows as n_0 increases. While the \downarrow and \downarrow^* configurations both emerge with the same energy $E_{\text{avg}} = 5.2 \text{ meV}$ at n_0^{onset} , the separation between these two grows up to 0.7 meV at $n_0 = 3 \times 10^5 \text{ cm}^{-1}$. The \uparrow configuration has the highest energy, exceeding that of the \downarrow solution by a constant value of 0.4 meV . However, below the n_0^{onset} threshold, \downarrow^* is forbidden, so the system assumes the \uparrow configuration. As a consequence, at n_0^{onset} , the ground state changes abruptly from a positive to a negative polarization. This spin-flip process is shown on the insets of figure 1(b). The polarization P_{gnd} of the ground state (top-left inset) drops suddenly from $+1$ (\uparrow configuration, dashed line) to -0.6 (\downarrow^* , dash-dotted line) at n_0^{onset} . The bottom-right inset displays the ratio n_{σ}/n_0 for the ground state of the system. Below n_0^{onset} , the system is in the \uparrow -configuration where n_{\uparrow} (solid line) exceeds n_{\downarrow} (dashed line). In this region, there is full spin-up polarization for concentrations below $4.51 \times 10^3 \text{ cm}^{-1}$ and above $1.92 \times 10^5 \text{ cm}^{-1}$. Between these two values n_{\uparrow} reaches a minimum at $n_0 = 0.54 \times 10^5 \text{ cm}^{-1}$ where only two-thirds of the electrons in the wire have spin-up. At n_0^{onset} , the system switches to the \downarrow^* configuration, for which $n_{\downarrow} > n_{\uparrow}$. At this spin-reversal point, three-fourths of the electrons have spin down, but as n_0 increases the difference between n_{\uparrow} and n_{\downarrow} decreases.

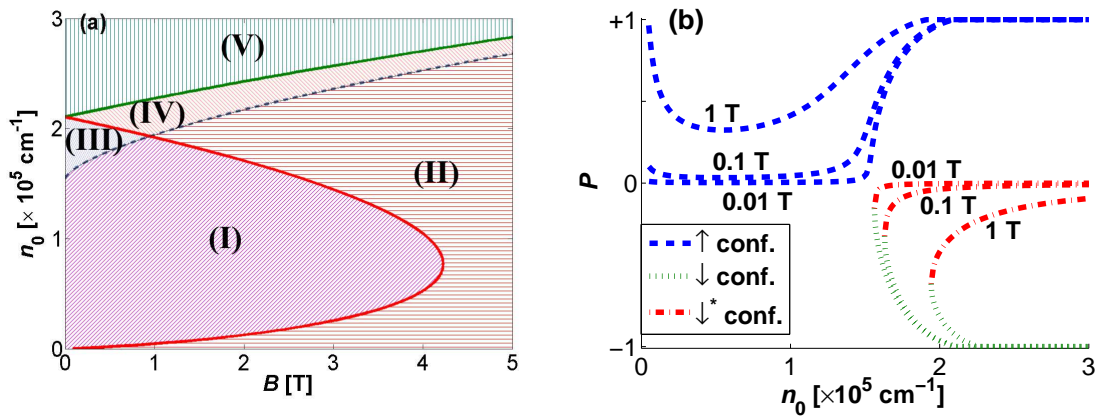


Figure 2. **Magnetic field dependence of the spin-polarized regimes.** (a) Magnetic phases diagram of the distinct spin-polarized regimes as a function of n_0 and B_x : (I) \uparrow configuration only, partially polarized; (II) \uparrow configuration only, fully polarized; (III) \uparrow (partial), \downarrow (partial), \downarrow^* (partial); (IV) \uparrow (full), \downarrow (partial), \downarrow^* (partial); (V) \uparrow (full), \downarrow (full), \downarrow^* (partial). (b) Polarization vs. n_0 for different magnetic field strengths. In all cases, $\hbar\omega_y = \hbar\omega_z = 2.0 \text{ meV}$ and $T = 0 \text{ K}$.

Figure 2(a) displays the various spin polarization regimes in the wire as both the magnetic fields and the concentrations are varied. Only the \uparrow configuration is present in regions (I) and (II), with either partial or full polarization, respectively. These two regions are separated by a solid, almost parabolically-shaped line. For $B_x > 4.22 \text{ T}$ the \uparrow configuration is completely polarized regardless of the concentration. The black dashed line corresponds to the minimum

concentration n_0^{onset} for the emergence of the \downarrow and \downarrow^* configurations. In regions (III) and (IV) the \uparrow configuration is, respectively, partially and fully polarized. Finally, region (V) lies above the topmost solid line that indicates the minimum concentration n_0^{full} for which the \downarrow configuration is fully polarized. In this region only the \downarrow^* configuration is partially polarized.

The presence of different polarization regimes in Fig. 2 is consistent with direct measurements of the spin polarization in quantum point contacts¹⁸ showing their variability as the magnetic field and concentration are changed. Furthermore, the sudden polarization reversal predicted in our model (Fig. 1(b)) also explains the abrupt rearrangement of the spin-up and spin-down levels under a strong in-plane magnetic field as observed by Graham et al²⁹ and previously interpreted as an exchange-driven magnetic phase transition^{29–31}. Indeed, at n_0^{onset} , the polarization of the ground state changes from positive to negative, so the energy of spin-up electrons suddenly rises above that of spin-down electrons, leading to the observed depopulation of the spin-up subband.

Figure 2(b) shows the effect of vanishing magnetic fields on the different spin polarizations in the wire, which evolve from a complex of configurations (\uparrow , \downarrow , and \downarrow^*) for $B_x \neq 0$ to a situation that sustains an unpolarized state co-existing with two degenerate and symmetrically spin-polarized regimes at high concentrations for $B_x = 0$. One can clearly see that the \uparrow spin polarization at low concentration, and the \downarrow^* spin polarization at high concentration collapse to an unpolarized configuration, while the \downarrow and \uparrow configurations are symmetric relative to each other. At the same time, the concentration threshold n_0^{onset} decreases to a lower common value for up- and down-spin polarization. As will be seen in Fig. 3(b), these two configurations are degenerate, characterized by a single Fermi level and equally probable, which is consistent with the absence of net magnetic moment in the wire.

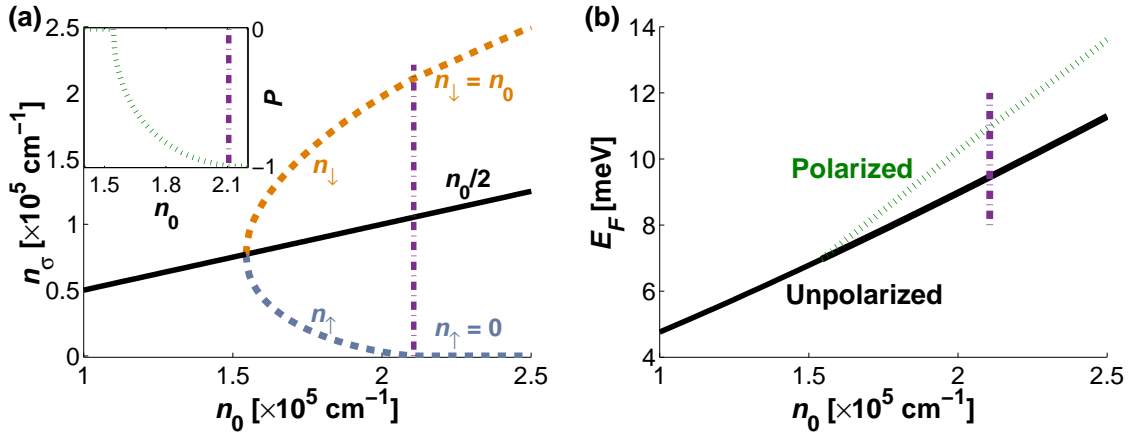


Figure 3. **Spin-polarized regimes at $B_x = 0$.** (a) Spin-polarized concentrations n_{\uparrow} and n_{\downarrow} vs. n_0 for the \downarrow configuration when $B_x = 0$. Inset: polarization of the \downarrow configuration vs. n_0 . (b) Fermi energy vs. n_0 for both the polarized (solid) and unpolarized (dotted) regimes. The vertical dash-dotted line marks the concentration for full polarization ($n_0^{\text{full}} = 2.1 \times 10^5 \text{ cm}^{-1}$). $\hbar\omega_y = \hbar\omega_z = 2.0 \text{ meV}$ and $T = 0 \text{ K}$.

The existence of spin polarization degeneracy when $B_x = 0$ can be shown from Eq. (2) where, besides from the trivial solution $\Delta n_{\sigma} = 0$ that corresponds to a spin-unpolarized electron density, one obtains the approximate solution for a non-zero Δn_{σ} in the limit $|\Delta n_{\sigma}| \ll n_0$ (see Supplementary Methods):

$$\Delta n_{\sigma} \approx \pm \sqrt{\frac{3}{\zeta_{ab}''(\pi n_0)} \left[a^* n_0 - \frac{\zeta_{ab}(\pi n_0)}{2\pi^2} \right]} \quad (3)$$

Here, $a^* = \frac{4\pi\epsilon\hbar^2}{q^2 m^*}$ is the effective Bohr radius and $\zeta_{ab}''(\pi n_0) = \left[\frac{d^2 \zeta_{ab}(p)}{dp^2} \right]_{p=\pi n_0}$. This solution is only valid for $n_0 \geq n_{0(B_x=0)}^{\text{onset}}$, where $n_{0(B_x=0)}^{\text{onset}}$ satisfies the identity obtained by setting $\Delta n_{\sigma} = 0$ in Eq. (3):

$$\frac{\zeta_{ab}(\pi n_{0(B_x=0)}^{\text{onset}})}{\pi n_{0(B_x=0)}^{\text{onset}}} = 2\pi a^* \quad (4)$$

Figure 3(a) is a plot of the spin-polarized concentrations in the wire for the \downarrow configuration ($n_{\downarrow} > n_{\uparrow}$) when $B_x = 0$. The solid line corresponds to the unpolarized case ($n_{\downarrow} = n_{\uparrow} = n_0/2$). The spin-polarized regime, represented by the

dashed curves, emerges at $n_0 = n_0^{\text{onset}} (= 1.54 \times 10^5 \text{ cm}^{-1})$. Above this threshold n_{\downarrow} continues to increase with n_0 until the wire becomes fully polarized ($n_{\downarrow} = n_0, n_{\uparrow} = 0$) for $n_0 \geq n_0^{\text{full}} (= 2.1 \times 10^5 \text{ cm}^{-1})$. The inset shows the polarization corresponding to this configuration as it changes from 0 at $n_0 = n_0^{\text{onset}}$ to -1 at $n_0 = n_0^{\text{full}}$.

Both spin-polarized configurations (\uparrow and \downarrow) have the same energy, which is generally higher than that of the unpolarized regime. This is shown in Fig. 3(b), which is a plot of the Fermi energy as a function of total concentration. At n_0^{onset} the Fermi energy is 6.97 meV for all configurations, but as n_0 increases the energy of the polarized configurations rises more rapidly, so at $n_0 = n_0^{\text{full}}$ the difference in energies between the two cases is about 1.5 meV. Therefore, at $T = 0 \text{ K}$, the ground state of the electrons in the wire will be unpolarized, in agreement with the Lieb-Mattis theorem²⁴. However, at higher temperatures the system can be excited to one of the spin-polarized regimes (which are indistinguishable from each other in the absence of a B -field), especially for concentrations close to n_0^{onset} when the energy difference between the polarized and unpolarized configurations is lower.

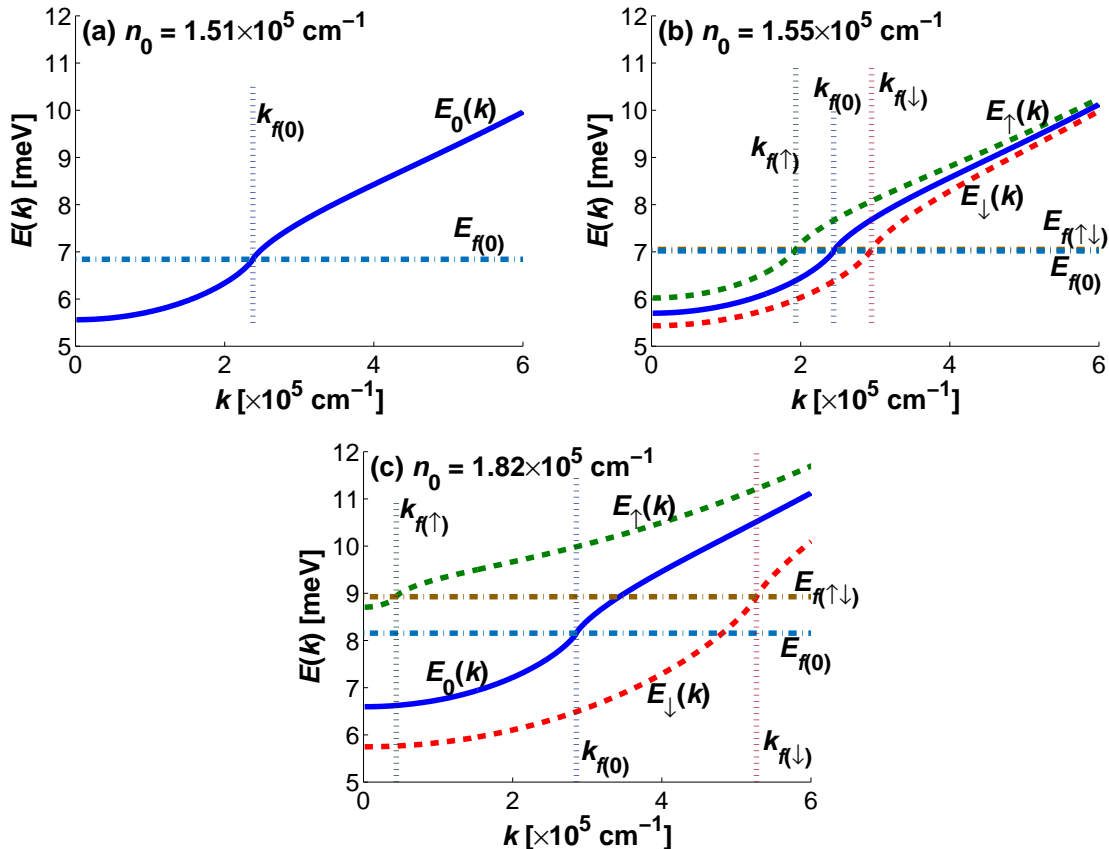


Figure 4. **Dispersion relation.** Energy vs. wavevector when $B_x = 0$, for three different concentrations: (a) just below the threshold for polarization; (b) just above the threshold; (c) significantly above the threshold. $\hbar\omega_y = \hbar\omega_z = 2.0 \text{ meV}$ and $T = 0 \text{ K}$. $E_0(k)$, $E_{f(0)}$ and $k_{f(0)}$ are, respectively, the energy and the Fermi wavevector in the unpolarized configuration, while $E_{\sigma}(k)$ and $k_{f(\sigma)}$ are the energy and the Fermi wavevector in the polarized configuration for electrons of spin $\sigma (= \uparrow, \downarrow)$.

The energy-momentum relation for spin-up and spin-down electrons at $B_x = 0$ is illustrated in Figures 4(a-c) for three different concentrations in the \downarrow configuration ($P < 0$). In all cases there is an inflection point at the Fermi wave vector caused by the exchange interaction, which indicates the presence of a maximum in the carrier velocity, a minimum in the 1D density of states, and an infinite effective mass. In Fig. 4(a), for which $n_0 < n_0^{\text{onset}} (= 1.54 \times 10^5 \text{ cm}^{-1})$, there is a single energy-momentum curve that, once the spin-polarized configuration emerges for $n_0 > n_0^{\text{onset}}$, splits into three curves, one of them above and another one below the unpolarized dispersion relation. In Fig. 4(b) the concentration is just above the threshold, so that both polarized concentrations exist below their Fermi level, which sits slightly higher than its unpolarized counterpart. In Fig. 4(c), the curve-splitting is more significant. The topmost dispersion relation, corresponding to spin-up electrons, is almost entirely above the spin-polarized Fermi level, which, in turn, is much higher than the unpolarized level. In both Fig. 4(b) and 4(c), the spin polarization tapers off at high wavevectors/energies, indicating that the effect weakens with carrier energy and concentration.

The emergence of density-dependent spin-polarized configurations is in agreement with previous experimental observations of a small conductance plateau around $0.5G_0 = e^2/h$ that appears in quantum wires for specific electron concentrations^{12–14}. According to our model, this plateau arises from the gap between the energies $E(k, \sigma)$ of spin-up and spin-down electrons in the polarized configurations, as shown in Fig. 4. Indeed, when the concentration is increased past the polarization threshold, e.g. by changing a gate voltage in a GaAs/AlGaAs heterostructure, one of the spin channels will gradually close, leading to a narrow step at e^2/h instead of $2e^2/h$. The predicted spin-polarized regime is an excited state, though, and the system is expected to fall back to the unpolarized configuration (which has a lower average energy; see Fig. 3(b)) as the density is increased, especially at low temperatures. The fact that the observed e^2/h feature is narrower than the $2e^2/h$ plateau and is enhanced with increasing temperature is consistent with previous conductance measurements^{13,14}.

The theoretical results also support the interpretation of a spin-polarized excited state as the origin of the anomalous conductance structure at $0.7G_0$ observed in quantum point contacts (QPCs)^{7,13,18}. Since the spin-polarized regimes occur in the high-energy excited states, the QPC potential barrier for these states is higher than that of the unpolarized configuration, reducing the conductance for those spin-polarized electrons. Furthermore, the electron concentration in spin-polarized configurations can be lowered by changing the gate voltage in the QPC heterostructure, inducing a further reduction of the conductance. These two facts are consistent with the temperature-enhanced pinning of the conductance near $0.7G_0$ at specific gate voltages.

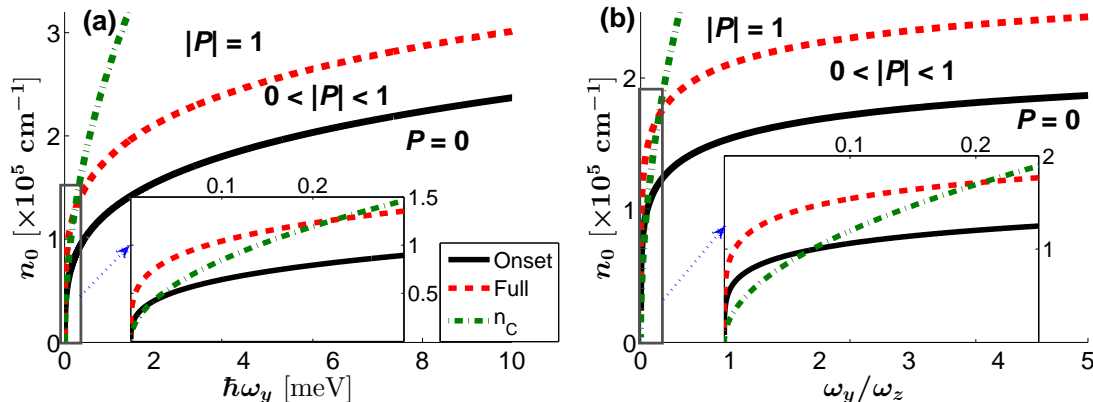


Figure 5. **Confinement dependence of the spin-polarized regimes.** Concentration n_0 at the onset of polarization (solid line) and when full polarization is achieved (dashed line) as a function of: (a) $\hbar\omega_y$ for the case $\hbar\omega_y = \hbar\omega_z \equiv \hbar\omega$; (b) ω_y/ω_z , with $\hbar\omega_z = 2$ meV. $B_x = 0$ and $T = 0$ in both cases. Insets: close-ups of regions $\hbar\omega < 0.3$ meV (in (a)) and $\omega_y/\omega_z < 0.25$ (in (b)) showing the maximum concentration n_C for which only one subband is occupied (dash-dotted line).

As mentioned before, the concentrations at the onset of polarization (n_0^{onset}) and at full polarization (n_0^{full}) also depend on the strength of the transverse confinement along the y - and z -directions, i.e. on the size of the cross-section of the wire. This is entirely due to the exchange interaction, since Eq. (2) predicts a confinement-independent threshold n_0^{onset} for non-interacting electrons ($\zeta_{ab}(p) \rightarrow 0$). Figure 5(a) displays the values of n_0^{onset} (solid line) and n_0^{full} (dashed line) as a function of the confinement strength $\hbar\omega_y$ for a wire with a circular cross section ($\hbar\omega_y = \hbar\omega_z \equiv \hbar\omega$) and at $B_x = 0$. If $\hbar\omega$ increases, both n_0^{onset} and n_0^{full} increase, although the rate of increase slows down and becomes almost constant when $\hbar\omega > 2$ meV. Furthermore, the range of n_0 for which partial polarization exists ($0 < |P| < 1$, corresponding to region (III) of Fig. 2(a)) becomes wider when the confinement is stronger. These data indicate that the wider the wire, i.e. the weaker the confinement, the lower the concentration for which polarization is possible, provided that the system remains in the extreme quantum limit. To satisfy this condition, the concentration must be smaller than a critical value $n_C = \frac{2}{\pi\hbar} \sqrt{2m^* (\hbar\omega_y)}$, since $\hbar\omega_y$ is the energy above the bottom of the first subband at which the second subband will start to become populated (when $\omega_y \leq \omega_z$). The inset shows a close-up of the n_0^{onset} and n_0^{full} curves for small values of $\hbar\omega$, as well as a plot of n_C (dash-dotted line). For $\hbar\omega \lesssim 0.02$ meV, $n_0^{\text{onset}} > n_C$ and the system is outside the scope of the model.

The effects of asymmetric confinement on n_0^{onset} and n_0^{full} are portrayed on Figure 5(b) as a function of the confinement strength ratio ω_y/ω_z for $\hbar\omega_z = 2$ meV, in the absence of a magnetic field. Both n_0^{onset} and n_0^{full} increase with the ratio, very rapidly for $\omega_y < \omega_z$ and at a much slower rate for $\omega_y > \omega_z$. This reflects the fact that the overlap function ζ_{ab} grows with stronger confinement (see Supplementary Figure S1). For instance, for $\hbar\omega_y = \hbar\omega_z = 10$ meV, $n_0^{\text{onset}} = 2.34 \times 10^5 \text{ cm}^{-1}$, whereas for $\hbar\omega_y = 10$ meV and $\hbar\omega_z = 2$ meV (corresponding to $\omega_y/\omega_z = 5$), $n_0^{\text{onset}} = 1.87 \times 10^5 \text{ cm}^{-1}$. As in Figure 5(a), the spin-polarized configurations are accessible until $n_0^{\text{onset}} > n_C$; as shown in the inset of Figure

5(b), this happens when $\omega_y/\omega_z \lesssim 0.068$ or $\hbar\omega_y \lesssim 0.14$ meV.

Our model shows that electron-electron interactions in quasi-1D systems with longitudinal magnetic fields lead to complex interweaved spin-polarized regimes which differ from previous works²¹, e.g. magnetic configurations opposite to those expected from pure Zeeman splitting in low-concentration quantum wires. These new results are the consequence of considering an exact 3D $1/r$ -Coulomb potential as opposed to a Dirac point potential^{21,31}, which enables us to include the interaction between electrons with parallel spins (prohibited with a Dirac interaction²¹) in the energy-momentum relation, Eq. (1). Specifically, at zero B -field, our theory shows that two symmetric and degenerate spin-polarized configurations exist for all values of carrier concentration (and Fermi energy) above a concentration threshold, even in the absence of spin-orbit interaction. The existence of the spin-polarized excited state in quasi-1D systems, more readily accessible as temperature is increased, is consistent with the emergence of a narrow conductance step near $0.5 \times 2e^2/h$ at low temperatures ($\sim 50 - 100$ mK)¹²⁻¹⁴, and its subsequent evolution into a broader feature near $0.7 \times 2e^2/h$ as the temperature is increased to a few kelvins in both quantum wires and quantum point contacts^{7,13,14,32}. The collective spin states described in our model also account for the observations of separate spin modes in coupled quantum wires that were originally attributed to Luttinger-liquid behavior^{10,11}. Our findings, however, result from the nonlinear nature of the energy dispersion relation as the particle concentration increases, thereby outlining the limitations of the low-energy, linear-dispersion Luttinger model³³. Such limitations are revealed through the observation of fast energy relaxation of particles in quantum wires, a process forbidden by Luttinger-liquid theory³⁴. Moreover, our results do not conform to the Wigner-crystal picture^{3,4} either, since it precludes the presence of spin-polarized states in the absence of a magnetic field. Indeed, in this picture, the condition for polarization is that the Zeeman energy $|U_Z| = g\mu_B B/2$ exceed the exchange energy $|U_{\text{exch}}|$ ³⁵, in contrast to our findings.

Furthermore, our theory highlights the importance of a full 3D approach to account for the sensitivity of the spin-polarized configurations to varying confinement strength and asymmetry. In this context, our model uses a pair of parabolic potentials for transverse confinement, which is suitable for elliptical wire cross-sections. It is, however, general and valid for other geometries, for which the overlap function $\zeta_{ab}(p)$, critical in setting the concentration threshold n_0^{onset} for the different spin-polarized regimes (Eq. (4)), would need to be evaluated with the corresponding wave functions. This is particularly relevant for spintronics applications, as it enables the design of quantum wires with specific spin-polarization characteristics by changing the shape and confinement of the 1D channel. For instance, in a GaAs/AlGaAs heterostructure, the desired range of polarizations can be set by choosing a suitable physical separation between the split gates and a specific acceptor density in GaAs. Subsequent fine-tuning of the polarization could be achieved by simply adjusting the split-gate potential bias.

Interestingly, our prediction that spin polarization is possible in symmetric quantum wires contrasts with the findings of Debray et al²⁵, whose experiments observed a spin-polarized current in a QPC only when the confinement potential was strongly asymmetric. It should, however, be pointed out that their QPC device is made with InAs, a material characterized by a strong intrinsic spin-orbit interaction. For this reason, the authors of that work attribute the emergence of spin polarization to a lateral spin-orbit coupling (which is a function of both the electron momentum and the confinement potential), as opposed to the Rashba spin-orbit interaction (which only depends on momentum). The extension of our model to incorporate both types of spin-orbit couplings is a topic of future investigation. However, the main objective of this work was to show that, even in the absence of such couplings, a variety of magnetic phases is achieved in quasi-1D systems by electric manipulation alone.

METHODS

We calculate the 1D energy-momentum relation within the unrestricted Hartree-Fock approximation, considering only the extreme quantum limit (i.e. when only the lowest-energy subband of the confinement potential is occupied), as described in the Supplementary Methods. All numerical calculations (e.g. solving for Δn_σ in Eq. (2)) were done using MATLAB.

ACKNOWLEDGMENTS

This work is supported by a grant from the Research Board at the University of Illinois at Urbana-Champaign (UIUC). A.X.S. also thanks the Department of Physics at UIUC for their continued support during his studies.

-
- * jleburto@illinois.edu
- ¹ C. Beenakker and H. van Houten, in *Semiconductor Heterostructures and Nanostructures*, Solid State Physics, Vol. 44, edited by H. Ehrenreich and D. Turnbull (Academic Press, Eindhoven, 1991) pp. 1 – 228.
 - ² S. A. Wolf, D. D. Awschalom, R. A. Buhrman, J. M. Daughton, S. von Molnár, M. L. Roukes, A. Y. Chtchelkanova, and D. M. Treger, *Science* **294**, 1488 (2001).
 - ³ K. A. Matveev, *Phys. Rev. Lett.* **92**, 106801 (2004).
 - ⁴ J. S. Meyer and K. A. Matveev, *J. Phys.: Condens. Matter* **21**, 023203 (2009).
 - ⁵ S. Tarucha, T. Honda, and T. Saku, *Solid State Commun.* **94**, 413 (1995).
 - ⁶ A. Yacoby, H. L. Stormer, N. S. Wingreen, L. N. Pfeiffer, K. W. Baldwin, and K. W. West, *Phys. Rev. Lett.* **77**, 4612 (1996).
 - ⁷ K. J. Thomas, J. T. Nicholls, M. Y. Simmons, M. Pepper, D. R. Mace, and D. A. Ritchie, *Phys. Rev. Lett.* **77**, 135 (1996).
 - ⁸ S. Nuttinck, K. Hashimoto, S. Miyashita, T. Saku, Y. Yamamoto, and Y. Hirayama, *Jpn. J. Appl. Phys.* **39**, L655 (2000).
 - ⁹ S. M. Cronenwett, H. J. Lynch, D. Goldhaber-Gordon, L. P. Kouwenhoven, C. M. Marcus, K. Hirose, N. S. Wingreen, and V. Umansky, *Phys. Rev. Lett.* **88**, 226805 (2002).
 - ¹⁰ O. M. Auslaender, H. Steinberg, A. Yacoby, Y. Tserkovnyak, B. I. Halperin, K. W. Baldwin, L. N. Pfeiffer, and K. W. West, *Science* **308**, 88 (2005).
 - ¹¹ Y. Jompol, C. J. B. Ford, J. P. Griffiths, I. Farrer, G. A. C. Jones, D. Anderson, D. A. Ritchie, T. W. Silk, and A. J. Schofield, *Science* **325**, 597 (2009).
 - ¹² B. E. Kane, G. R. Facer, A. S. Dzurak, N. E. Lumpkin, R. G. Clark, L. N. Pfeiffer, and K. W. West, *Appl. Phys. Lett.* **72**, 3506 (1998).
 - ¹³ K. J. Thomas, J. T. Nicholls, M. Pepper, W. R. Tribe, M. Y. Simmons, and D. A. Ritchie, *Phys. Rev. B* **61**, R13365 (2000).
 - ¹⁴ D. J. Reilly, T. M. Buehler, J. L. O'Brien, A. R. Hamilton, A. S. Dzurak, R. G. Clark, B. E. Kane, L. N. Pfeiffer, and K. W. West, *Phys. Rev. Lett.* **89**, 246801 (2002).
 - ¹⁵ A. A. Starikov, I. I. Yakimenko, and K.-F. Berggren, *Phys. Rev. B* **67**, 235319 (2003).
 - ¹⁶ P. Havu, M. J. Puska, R. M. Nieminen, and V. Havu, *Phys. Rev. B* **70**, 233308 (2004).
 - ¹⁷ A. D. Klironomos, J. S. Meyer, and K. A. Matveev, *Europhys. Lett.* **74**, 679 (2006).
 - ¹⁸ L. P. Rokhinson, L. N. Pfeiffer, and K. W. West, *Phys. Rev. Lett.* **96**, 156602 (2006).
 - ¹⁹ K.-F. Berggren and I. I. Yakimenko, *J. Phys.: Condens. Matter* **20**, 164203 (2008).
 - ²⁰ A. P. Micolich, *J. Phys.: Condens. Matter* **23**, 443201 (2011).
 - ²¹ H. Lind, I. I. Yakimenko, and K.-F. Berggren, *Phys. Rev. B* **83**, 075308 (2011).
 - ²² K. Hirose, Y. Meir, and N. S. Wingreen, *Phys. Rev. Lett.* **90**, 026804 (2003).
 - ²³ T. Rejec and Y. Meir, *Nature* **442**, 900 (2006).
 - ²⁴ E. Lieb and D. Mattis, *Phys. Rev.* **125**, 164 (1962).
 - ²⁵ P. Debray, S. M. S. Rahman, J. Wan, R. S. Newrock, M. Cahay, A. T. Ngo, S. E. Ulloa, S. T. Herbert, M. Muhammad, and M. Johnson, *Nat. Nanotechnol.* **4**, 759 (2009).
 - ²⁶ J. Wan, M. Cahay, P. Debray, and R. S. Newrock, *J. Nanoelectron. Optoelectron.* **6**, 95 (2011).
 - ²⁷ A. X. Sánchez and J.-P. Leburton, *Phys. Rev. B* **88**, 075305 (2013).
 - ²⁸ K. Hess, *Advanced Theory of Semiconductor Devices* (Wiley-IEEE Press, New York, 2000).
 - ²⁹ A. C. Graham, D. L. Sawkey, M. Pepper, M. Y. Simmons, and D. A. Ritchie, *Phys. Rev. B* **75**, 035331 (2007).
 - ³⁰ K.-F. Berggren, P. Jaksch, and I. Yakimenko, *Phys. Rev. B* **71**, 115303 (2005).
 - ³¹ A. Lassl, P. Schlagheck, and K. Richter, *Phys. Rev. B* **75**, 045346 (2007).
 - ³² A. Kristensen, H. Bruus, A. E. Hansen, J. B. Jensen, P. E. Lindelof, C. J. Marckmann, J. Nygård, C. B. Sørensen, F. Beuscher, A. Forchel, and M. Michel, *Phys. Rev. B* **62**, 10950 (2000).
 - ³³ A. Imambekov, T. L. Schmidt, and L. I. Glazman, *Rev. Mod. Phys.* **84**, 1253 (2012).
 - ³⁴ G. Barak, H. Steinberg, L. N. Pfeiffer, K. W. West, L. Glazman, F. von Oppen, and A. Yacoby, *Nat. Phys.* **6**, 489 (2010).
 - ³⁵ V. V. Deshpande, M. Bockrath, L. I. Glazman, and A. Yacoby, *Nature* **464**, 209 (2010).

SUPPLEMENTARY METHODS

Variational calculation of the 1D energy-momentum relation

In a longitudinal magnetic field $\vec{B} = B_x \hat{x}$, with the gauge set to $\vec{A} = B_x y \hat{z}$, the Schrödinger equation within the unrestricted Hartree-Fock approximation²⁷ reads

$$-\frac{\hbar^2}{2m^*} \nabla^2 \psi_{\{i\}}(\vec{r}) + \left[U_{\text{conf}}(y, z) + \frac{1}{2} m^* \omega_B^2 y^2 + i \hbar \omega_B y \frac{\partial}{\partial z} + U_{\text{el}}(\vec{r}) \right] \psi_{\{i\}}(\vec{r}) + \hat{U}_{\text{exch}}[\psi_{\{i\}}(\vec{r})] + U_Z \psi_{\{i\}}(\vec{r}) = E_{\{i\}} \psi_{\{i\}}(\vec{r}) \quad (\text{S1})$$

Here, $\{i\} = \{i_x, i_y, i_z, \sigma_i = \pm \frac{1}{2}\}$ are the quantum numbers associated with the eigenenergies $E_{\{i\}}$, $\omega_B = \frac{qB_0}{m^*}$ is the cyclotron frequency, q is the electron charge, m^* is the effective mass, $U_{\text{conf}}(y, z) = \frac{1}{2} m^* \omega_y^2 y^2 + \frac{1}{2} m^* \omega_z^2 z^2$ is the lateral confinement potential, $U_Z = g \mu_B B_x \sigma$ is the Zeeman energy term, g is the effective electron g -factor, $\mu_B = \frac{q\hbar}{2m^*}$ is the Bohr magneton in the wire, and U_{el} and \hat{U}_{exch} are the Hartree and exchange terms, respectively²⁷.

In the extreme quantum limit, i.e. when only the lowest-energy subband of the confinement potential is occupied, we take the expectation value of the left-hand side of Eq. (S1), using the trial wavefunction

$$\psi_{k_x}(\vec{r}) = \frac{1}{\sqrt{L_x}} e^{ik_x x} \left(\frac{a^{1/2}}{\pi^{1/4}} e^{-a^2 y^2 / 2} \right) \left(\frac{b^{1/2}}{\pi^{1/4}} e^{-b^2 z^2 / 2} \right) \quad (\text{S2})$$

where $a = \sqrt{\frac{m^* \omega_y}{\hbar}}$ and $b = \sqrt{\frac{m^* \omega_z}{\hbar}}$. In the absence of electron-electron interactions and for zero magnetic field, this wavefunction corresponds to the exact ground state of Eq. (S1). Then, one obtains the following expression for the single-particle energy:

$$E(k_x, \sigma) = \frac{\hbar^2 k_x^2}{2m^*} + \frac{1}{2} \hbar \omega_y + \frac{1}{2} \hbar \omega_z + \frac{1}{4} \left(\frac{\omega_B}{\omega_y} \right) \hbar \omega_B + g \mu_B B_x \sigma + U_{\text{el}}[n_0] + U_{\text{exch}}(k_x, \sigma) \quad (\text{S3})$$

The expectation values U_{el} and U_{exch} are²⁷

$$U_{\text{el}}[n_0] = \frac{q^2 \zeta_{ab}(0)}{16\pi\epsilon} n_0$$

$$U_{\text{exch}}(k_x, \sigma) = -\frac{q^2}{32\pi^2\epsilon} \int_{-\infty}^{+\infty} dp_x \zeta_{ab}(p_x - k_x) f_T[E(p_x, \sigma)]$$

where $n_0 = \frac{1}{2\pi} \sum_{\sigma} \int_{-\infty}^{+\infty} dp f_T[E(p, \sigma)] = \sum_{\sigma} n_{\sigma}$ is the total electron density in the wire; $f_T[E] = \{1 + \exp[(E - \mu)/k_B T]\}^{-1}$ is the Fermi-Dirac distribution for a chemical potential μ ; and $\zeta_{ab}(p)$, a form function which is specific to the wavefunction shown in Eq. (S2), is

$$\zeta_{ab}(p) = 8 \left(\frac{a}{b} \right) \int_0^{+\infty} dt \frac{t \exp(-t^2/2)}{\sqrt{\left(\frac{p}{b}\right)^2 + t^2} \sqrt{\left(\frac{p}{b}\right)^2 + \left(\frac{a}{b}\right)^2 t^2}} \quad ; \quad (\text{S4})$$

$\zeta_{ab}(p)$ is a monotonically-decreasing function of p and it increases with increasing a and b (i.e. with stronger confinement strengths). A plot of $\zeta_{ab}(p)$ for different values of a and b is shown in Supplementary Figure S1.

At zero temperature, μ is equal to the Fermi energy E_f and $f_T(E) = \theta(E_f - E(k)) = \theta(k_{f(\sigma)} - |k|)$, where $k_{f(\sigma)}$ is the spin-dependent Fermi wavevector such that $E(k_{f(\sigma)}) = E_f$. Then, the exchange term turns into

$$U_{\text{exch}}(k_x, \sigma) = -\frac{q^2}{32\pi^2\epsilon} \int_{-k_{f(\sigma)} + k_x}^{+k_{f(\sigma)} + k_x} dp \zeta_{ab}(p)$$

Calculation of Δn_σ , n_0^{onset} and n_0^{full}

At $T = 0$, when the concentrations of both spin-up and spin-down electrons are positive, they are directly proportional to a spin-dependent Fermi wavevector via the relation $k_{f(\sigma)} = \pi n_\sigma$. Thus, the Fermi energy $E_f = E(k_{f(\sigma)})$ can be written in terms of n_σ and n_0 :

$$E_f(n_\sigma) = \frac{\hbar^2 \pi^2 n_\sigma^2}{2m^*} + \frac{1}{2} \hbar \omega_y + \frac{1}{2} \hbar \omega_z + \frac{1}{4} \left(\frac{\omega_B}{\omega_y} \right) \hbar \omega_B \\ + g \mu_B B_x \sigma + \frac{q^2 \zeta_{ab}(0)}{16\pi\epsilon} n_0 - \frac{q^2}{32\pi^2\epsilon} \int_{-\pi n_0/2 + \pi n_\sigma}^{+\pi n_0/2 + \pi n_\sigma} dp \zeta_{ab}(p)$$

n_σ can be written in terms of the average concentration $n_0/2$ and the deviation from this average value $\Delta n_\sigma \equiv n_\sigma - n_0/2$ (so $\Delta n_{-\sigma} = -\Delta n_\sigma$). Then, since E_f is spin-independent, we get $E_f(n_\sigma) = E_f(n_{-\sigma})$. From this equation one obtains the following expression, which corresponds to Equation (2) in the main text:

$$\frac{\pi^2}{2} n_0 \Delta n_\sigma + \sigma \frac{qgB_x}{2\hbar} - \frac{q^2 m^*}{64\pi^2 \epsilon \hbar^2} \int_{2\pi(n_0/2 - \Delta n_\sigma)}^{2\pi(n_0/2 + \Delta n_\sigma)} dp \zeta_{ab}(p) \equiv F(\Delta n_\sigma; n_0) = 0 \quad (\text{S5})$$

For non-interacting electrons (i.e. when the overlap function $\zeta_{ab}(p)$ vanishes), the magnetic field induces a Zeeman splitting between spin-up and spin-down electrons. For $n_0 \geq n_B \equiv \sqrt{\frac{q|gB_x|}{\pi^2 \hbar}}$, the (unique) solution to Eq. (S5) reduces to $n_\sigma = \frac{n_0}{2} \left[1 - \left(\frac{n_B}{n_0} \right)^2 \text{sign}(gB_x \sigma) \right]$. However, for $n_0 < n_B$, if $\text{sign}(gB_x) > (<) 0$, this last equation yields $n_{\uparrow(\downarrow)} < 0$, which must then be set to zero, so the wire exhibits full spin-down (up) polarization ($n_{\downarrow(\uparrow)} = n_0$).

In the general case of interacting electrons ($\zeta_{ab}(p) \neq 0$), and if the concentration is low, Eq. (S5) yields only one solution for Δn_σ in terms of n_0 . However, if n_0 exceeds a certain threshold value n_0^{onset} then two additional solutions, or spin configurations, are possible. This is illustrated in Supplementary Figure S2, which is a plot of $F(\Delta n_\sigma; n_0)$ (the left-hand side of Eq. (S5)) versus Δn_\uparrow for a few values of n_0 . As in Figure 1 in the main text, $B_x = 1$ T and $\hbar \omega_y = \hbar \omega_z = 2$ meV, yielding $n_0^{\text{onset}} = 1.94 \times 10^5 \text{ cm}^{-1}$. The solutions to Eq. (S5) correspond to the crossings of the curves with the x -axis (dotted line). When the concentration is below n_0^{onset} (dashed line), there is a single positive solution for Δn_\uparrow , which corresponds to the “ \uparrow ” configuration in Fig. 1. Meanwhile, when $n_0 \geq n_0^{\text{onset}}$ (dash-dotted line), two additional negative solutions are possible; they correspond to the “ \downarrow ” and “ \downarrow^* ” configurations of Fig. 1. For $n_0 = n_0^{\text{onset}}$ (solid line), the slope of the function $F(\Delta n_\uparrow; n_0)$ is zero at the value of Δn_\uparrow for which the negative solution emerges. Thus, n_0^{onset} and the corresponding Δn_σ are the solutions of the pair of equations $F(\Delta n_\sigma; n_0) = 0$ and $\frac{\partial F(\Delta n_\sigma; n_0)}{\partial \Delta n_\sigma} = 0$.

In the limit $|\Delta n_\sigma| \ll n_0$, one can expand the integral in Eq. (S5) as a series in Δn_σ . Up to the third order, this results in a cubic equation:

$$\frac{\pi^2}{2} n_0 \Delta n_\sigma + \sigma \frac{qgB_x}{2\hbar} - \frac{q^2 m^*}{16\pi^2 \epsilon \hbar^2} \left\{ \pi \Delta n_\sigma \zeta_{ab}(\pi n_0) + \frac{2}{3} (\pi \Delta n_\sigma)^3 \zeta_{ab}''(\pi n_0) + \dots \right\} = 0$$

Here, $\zeta_{ab}''(\pi n_0) = \left[\frac{d^2 \zeta_{ab}(p)}{dp^2} \right]_{p=\pi n_0}$. This leads to the approximate expression for the non-zero values of Δn_σ when $B_x = 0$ (Eq. (3) in the main text):

$$\Delta n_\sigma \approx \pm \sqrt{\frac{3}{\zeta_{ab}''(\pi n_0)} \left[a^* n_0 - \frac{\zeta_{ab}(\pi n_0)}{2\pi^2} \right]}$$

where $a^* \equiv \frac{4\pi\epsilon\hbar^2}{q^2 m^*}$ is the effective Bohr radius. However, this solution is only valid if the argument inside the square root is non-negative, which means that the minimum concentration $n_{0(B_x=0)}^{\text{onset}}$ for the emergence of the non-zero solution must satisfy the identity

$$\frac{\zeta_{ab}(\pi n_{0(B_x=0)}^{\text{onset}})}{\pi n_{0(B_x=0)}^{\text{onset}}} = 2\pi a^*$$

As n_0 increases above n_0^{onset} , Δn_σ will continue to increase until the wire is completely spin-polarized at a concentration n_0^{full} . Setting $\Delta n_\sigma = \pm n_0/2$ in Eq. (S5) gives the following equation for n_0^{full} , the value of n_0 for which full spin polarization is achieved:

$$\frac{\pi^2}{4} (n_0^{\text{full}})^2 - \frac{q^2 m^*}{64\pi^2 \epsilon \hbar^2} \int_0^{2\pi n_0^{\text{full}}} dp \zeta_{ab}(p) = -\text{sign}(\sigma \Delta n_\sigma) \frac{qgB_x}{4\hbar}$$

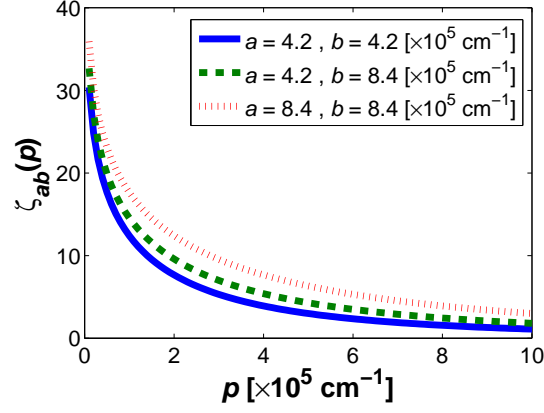


Figure S1. $\zeta_{ab}(p)$ as a function of p for different values of a and b .

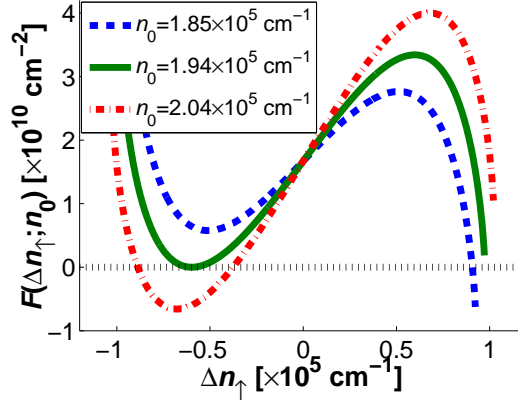


Figure S2. $F(\Delta n_\uparrow; n_0)$ vs. Δn_\uparrow for different n_0 , with $B_x = 1$ T and $\hbar\omega_y = \hbar\omega_z = 2$ meV.